Rensselaer

A Stable Partitioned FSI Algorithm for Incompressible Flow and Deforming Beams

Longfei Li

Rensselaer Polytechnic Institute

In collaboration with:
W. D. Henshaw, J. W. Banks and D. W. Schwendeman

October 19th, 2016
13th Symposium on Overset Composite Grids and Solution Technology
Future of Flight Aviation Center, Mukilteo, WA USA

Outline

- Introduction
- Governing Equations
- Added Mass Partition (AMP) Scheme
- Stability Analysis
- Numerical Results
- Summary

Introduction

Fluid-structure interaction (FSI) problems are important in many areas of engineering and applied science, such as modeling blood flow, aircraft, undersea cables and wind turbines, etc. In this talk, we focus on solving problems involving fluid interaction with a beam/shell.

Numerical Methods

- Monolithic Methods
  - treat everything as a large system of evolution equations
  - advance the solutions together
  - less efficient
  - less flexible
- Partitioned Methods
  - reuse existing computational codes
  - successfully applied in many cases
  - stability issue arises for light beam
  - referred to as Added-Mass Instability

Introduction

Fluid-structure interaction (FSI) problems are important in many areas of engineering and applied science, such as modeling blood flow, aircraft, undersea cables and wind turbines, etc. In this talk, we focus on solving problems involving fluid interaction with a beam/shell.

Numerical Methods

- Monolithic Methods
  - treat everything as a large system of evolution equations
  - advance the solutions together
  - less efficient
  - less flexible
- Partitioned Methods
  - reuse existing computational codes
  - successfully applied in many cases
  - stability issue arises for light beam
  - referred to as Added-Mass Instability

Origin of Added-Mass Instabilities

in a vacuum

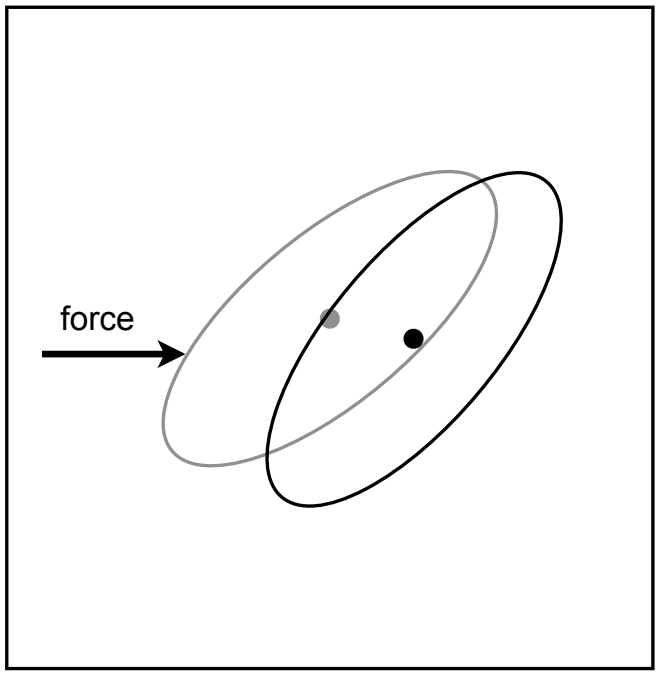

Body simply moves according to Newton's laws of motion

in a fluid

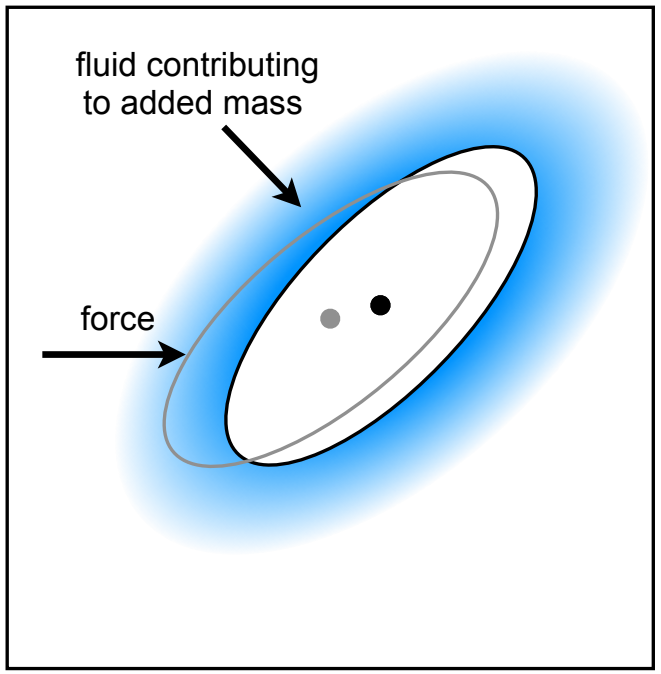

Body must displace and entrain fluid to move and therefore appears more massive than in vacuum ... the so called "added mass"

Partial Fixes of Added-Mass Instability

- Robin-Robin (mixed) boundary conditions with coefficients determined from simplified known solutions
- Interface artificial compressibility, fictitious pressure and fictitious mass
- Time-split interface conditions
- Semi-monolitic, approximate factorizations, Newton type schemes and fixed point iterations (Aitken accelerated)

References

Causin *et al.* (2005), Forster *et al.* (2007), van Brummelen (2009), Badia *et al.* (2008), Astorino *et al.* (2009), Degroote *et al.* (2009), Guidoboni *et al.* (2009), Fernandez (review, 2011), Gretarsson *et al.* (2011), Baek & Karniadakis (2012), Nobile & Vergara (2012), Yu *et al.* (2013), Bukac *et al.* (2013), Fernandez *et al.* (2014), Fernandez & Landajuela (2014), . . .

Introduction

Traditional Scheme with Sub-Iterations (TS-SI)

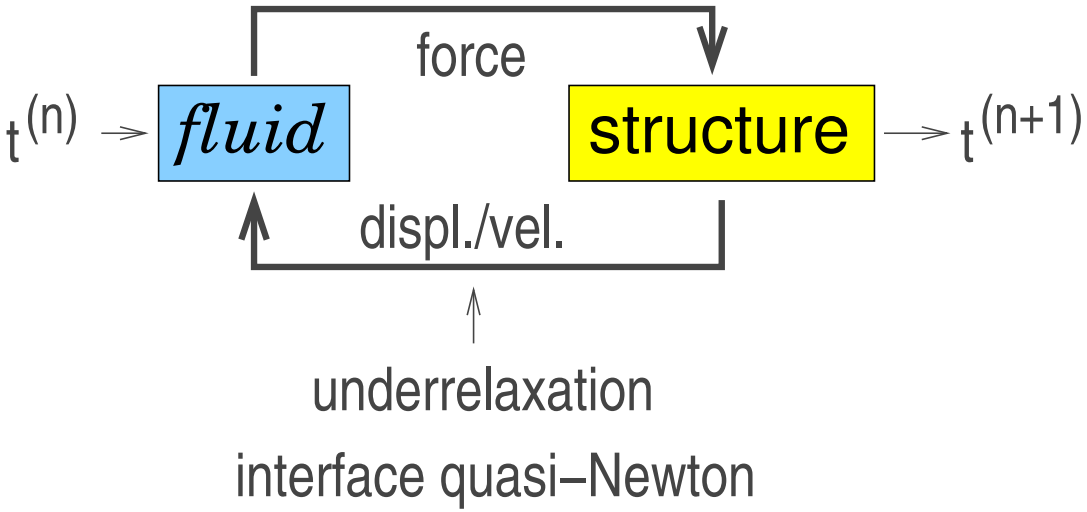

diagram from
Keyes et. al. 2012

- advance solid (apply fluid forces to the solid)
- advance fluid (using interface velocity/position from the solid)
- possibly iterate with under-relaxation to convergence for light solid

Introduction

Turek & Hron Benchmark Problem

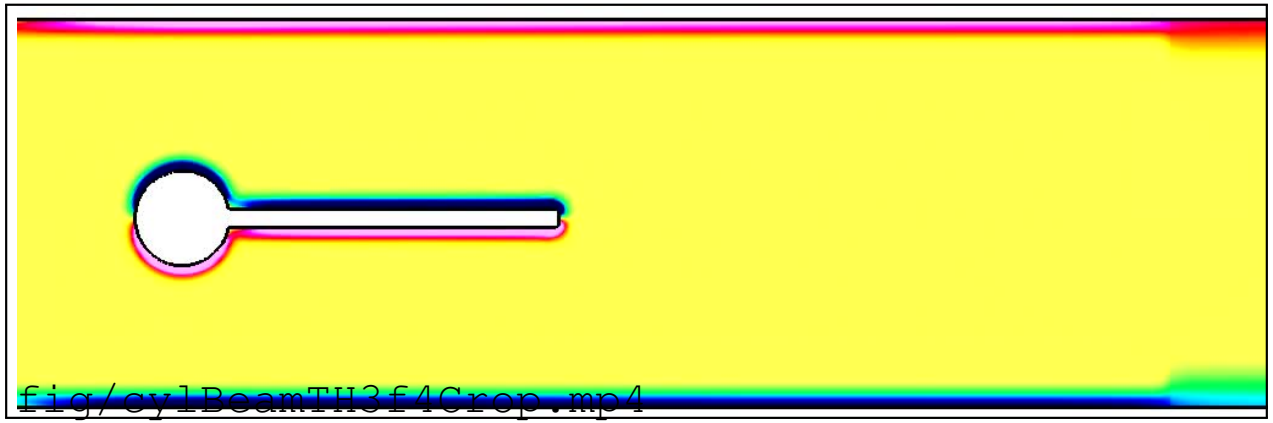

Two Beams in A channel

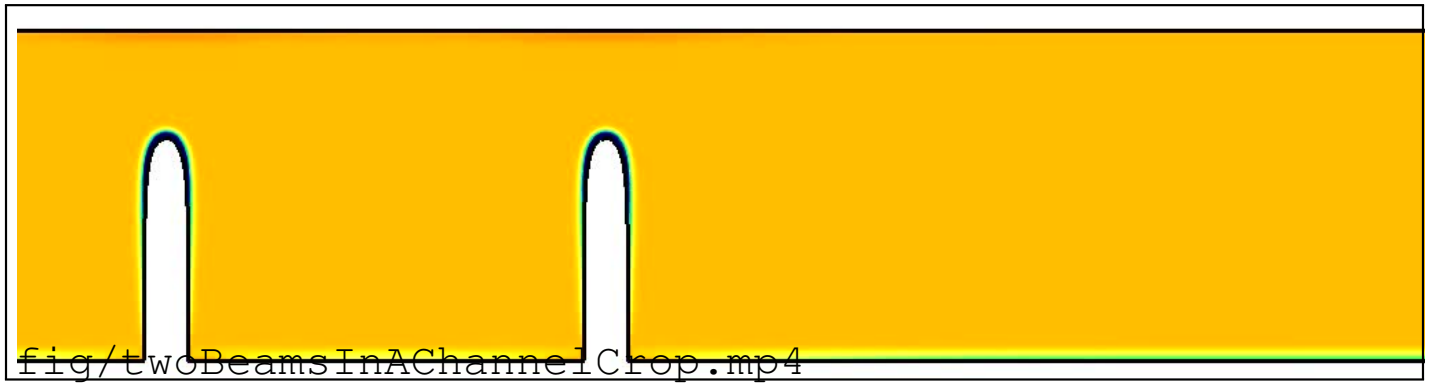

- Simulations conducted using TP-IS Scheme.
- TP scheme works well for heavy beam ($\rho_s/\rho_f = 1000$), while sub-iterations have to be added to stabilize the scheme for lighter beams.

Governing Equations

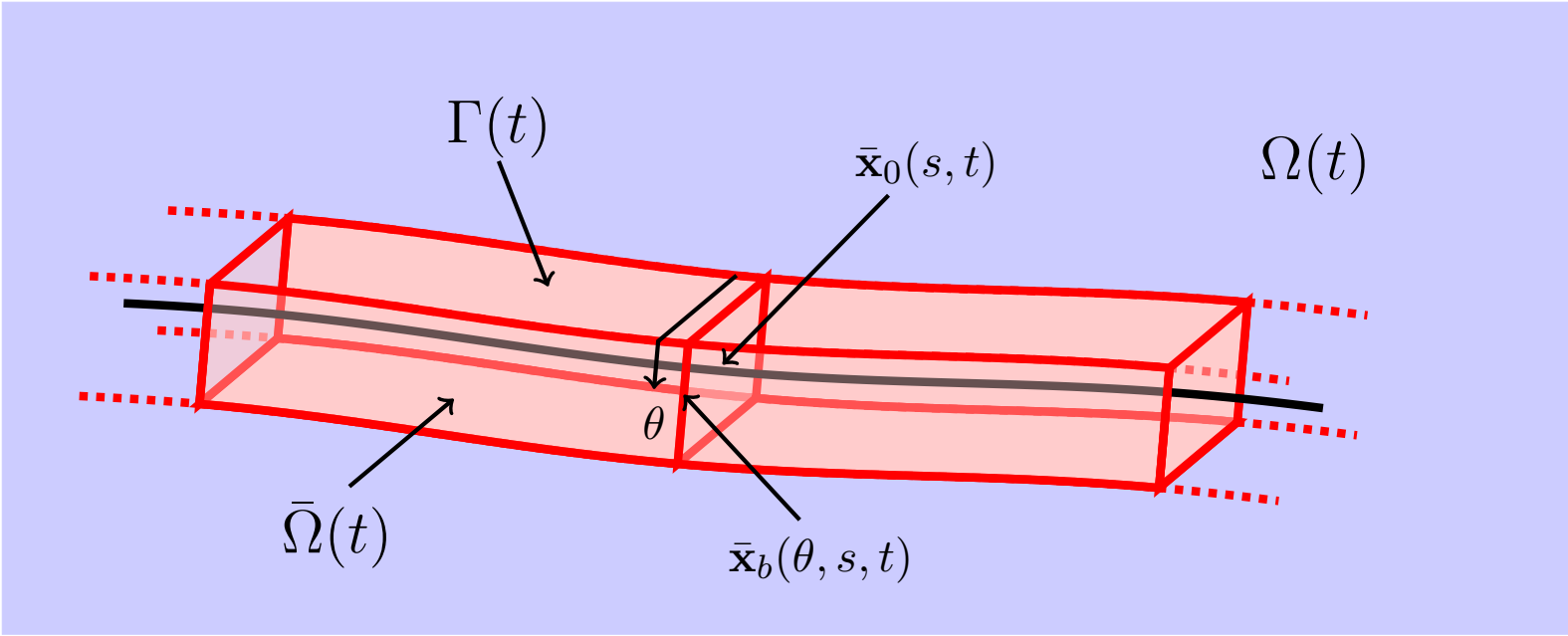

Fluid: $\mathbf{x} \in \Omega(t)$

$$\frac{\partial \mathbf{v}}{\partial t} + (\mathbf{v}\cdot\nabla)\mathbf{v} = \frac{1}{\rho}\nabla\cdot\boldsymbol{\sigma}, \quad \nabla\cdot\mathbf{v} = 0,$$

$$\boldsymbol{\sigma} = -p\mathbf{I} + \boldsymbol{\tau}, \quad \boldsymbol{\tau} = \mu\left[\nabla\mathbf{v} + (\nabla\mathbf{v})^T\right],$$

Beam: $\mathbf{s} \in \bar{\Omega}$

$$\bar{\rho}\bar{A}\frac{\partial^2\bar{\mathbf{u}}}{\partial t^2} = \bar{\mathbf{L}}(\bar{\mathbf{u}},\bar{\mathbf{v}}) + \bar{\mathbf{f}}(\mathbf{s},t)$$

$$\bar{\mathbf{f}}(\mathbf{s},t) = -\int_{\bar{\mathcal{P}}} (\boldsymbol{\sigma}\mathbf{n})(\hat{\theta},\mathbf{s},t)\, d\hat{\theta}$$

Interface: $\mathbf{v}(\bar{\mathbf{x}}_b(\theta,\mathbf{s},t),t) = \bar{\mathbf{v}}_b(\theta,\mathbf{s},t)$

Governing Equations

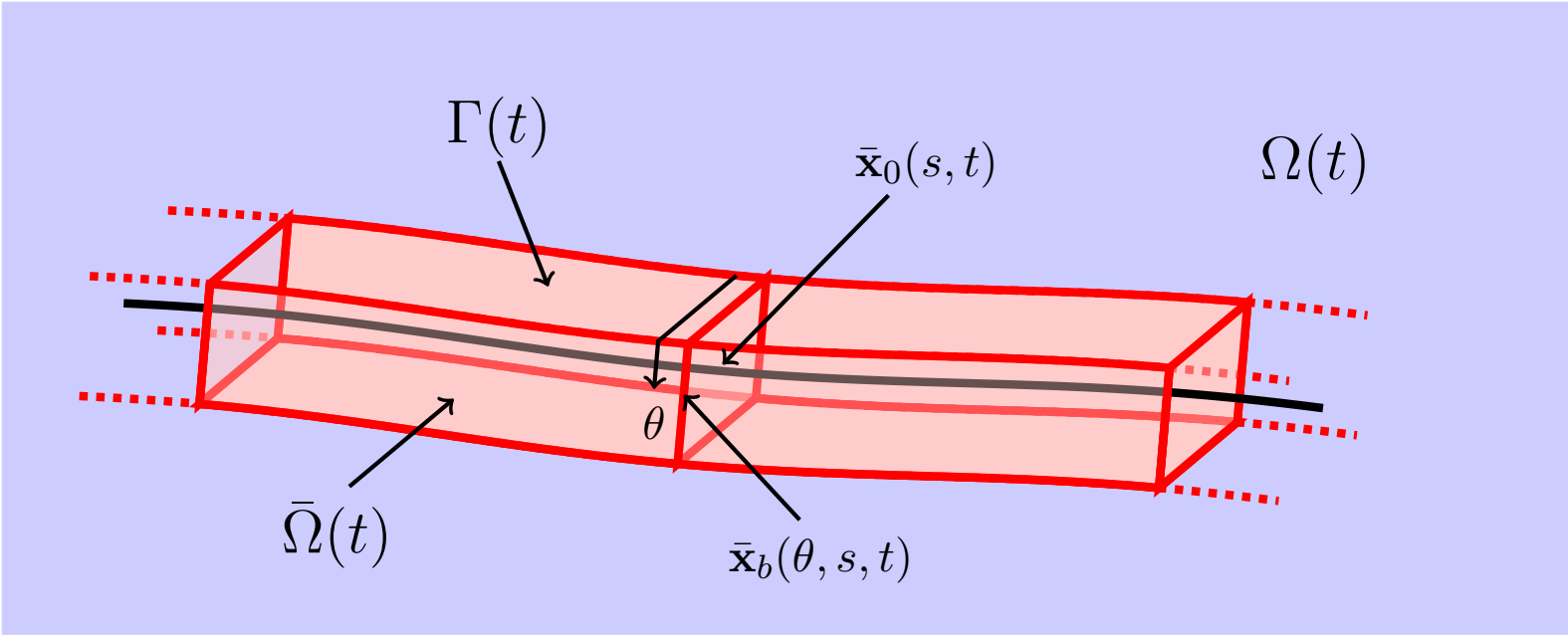

Fluid: $\mathbf{x} \in \Omega(t)$

$$\frac{\partial \mathbf{v}}{\partial t} + (\mathbf{v}\cdot\nabla)\mathbf{v} = \frac{1}{\rho}\nabla\cdot\boldsymbol{\sigma}, \quad \nabla\cdot\mathbf{v} = 0,$$

$$\boldsymbol{\sigma} = -p\mathbf{I} + \boldsymbol{\tau}, \quad \boldsymbol{\tau} = \mu\left[\nabla\mathbf{v} + (\nabla\mathbf{v})^T\right],$$

Beam: $\mathbf{s} \in \bar{\Omega}$

$$\bar{\rho}\bar{A}\frac{\partial^2\bar{\mathbf{u}}}{\partial t^2} = \bar{\mathbf{L}}(\bar{\mathbf{u}},\bar{\mathbf{v}}) + \bar{\mathbf{f}}(\mathbf{s},t)$$

$$\bar{\mathbf{f}}(\mathbf{s},t) = -\int_{\bar{\mathcal{P}}} (\boldsymbol{\sigma}\mathbf{n})(\hat{\theta},\mathbf{s},t)\, d\hat{\theta}$$

Interface: $\mathbf{v}(\bar{\mathbf{x}}_b(\theta,\mathbf{s},t),t) = \bar{\mathbf{v}}_b(\theta,\mathbf{s},t)$

AMP Scheme

We derive the AMP scheme by matching the accelerations of fluid and beam at the interface $\Gamma(t)$:

$$\frac{D}{Dt}\mathbf{v}(\bar{\mathbf{x}}_b(\theta,\mathbf{s},t),t) = \frac{\partial^2 \bar{\mathbf{u}}}{\partial t^2}(\mathbf{s},t) + \frac{\partial}{\partial t}\bar{\mathbf{w}}(\theta,\mathbf{s},t)$$

$$\Rightarrow \frac{\bar{\rho}\bar{A}}{\rho}\nabla\cdot\boldsymbol{\sigma}(\bar{\mathbf{x}}_b(\theta,\mathbf{s},t),t) = \bar{\mathbf{L}}(\bar{\mathbf{u}},\bar{\mathbf{v}}) + \bar{\mathbf{f}}(\mathbf{s},t) + \bar{\rho}\bar{A}\frac{\partial}{\partial t}\bar{\mathbf{w}}(\theta,\mathbf{s},t)$$

Remark: $\bar{\mathbf{w}}(\theta,\mathbf{s},t)$ is the finite-thickness correction of the beam velocity.

AMP Interface Condition

$$\int_{\bar{\mathcal{P}}}(\boldsymbol{\sigma}\mathbf{n})(\hat{\theta},\mathbf{s},t)\,d\hat{\theta} + \frac{\bar{\rho}\bar{A}}{\rho}\nabla\cdot\boldsymbol{\sigma}(\bar{\mathbf{x}}_b(\theta,\mathbf{s},t),t) = \bar{\mathbf{L}}(\bar{\mathbf{u}},\bar{\mathbf{v}}) + \bar{\rho}\bar{A}\frac{\partial}{\partial t}\bar{\mathbf{w}}(\theta,\mathbf{s},t)$$

Partitioned Schemes Using the AMP Condition

$$\int_{\bar{\mathcal{P}}}(\boldsymbol{\sigma}\mathbf{n})(\hat{\theta},\mathbf{s},t)\,d\hat{\theta} + \frac{\bar{\rho}\bar{A}}{\rho}\nabla\cdot\boldsymbol{\sigma}(\bar{\mathbf{x}}_b(\theta,\mathbf{s},t),t) = \bar{\mathbf{L}}(\bar{\mathbf{u}}^{(p)},\bar{\mathbf{v}}^{(p)}) + \bar{\rho}\bar{A}\frac{\partial}{\partial t}\bar{\mathbf{w}}^{(p)}(\theta,\mathbf{s},t)$$

where $\bar{\mathbf{u}}^{(p)}$, $\bar{\mathbf{v}}^{(p)}$ and $\bar{\mathbf{w}}^{(p)}$ are predicted solid variables.

AMP Scheme

The fluid equations are solved in the velocity-pressure formulation using a split-step scheme. [Henshaw & Petersson, 2001].

$$\frac{\partial \mathbf{v}}{\partial t} + (\mathbf{v}\cdot\nabla)\mathbf{v} = \frac{1}{\rho}\nabla\cdot\boldsymbol{\sigma}, \qquad \mathbf{x}\in\Omega$$

$$\Delta p = -\rho\nabla\mathbf{v} : (\nabla\mathbf{v})^T, \qquad \mathbf{x}\in\Omega$$

$$\nabla\cdot\mathbf{v} = 0, \qquad \mathbf{x}\in\partial\Omega$$

AMP Velocity Condition (tangential component of AMP condition)

$$\mathbf{t}_m^T\left[\int_{\bar{\mathcal{P}}}(\boldsymbol{\tau}\mathbf{n})(\hat{\theta},\mathbf{s},t)\,d\hat{\theta} + \frac{\mu\bar{\rho}\bar{A}}{\rho}\Delta\mathbf{v}\right] = \mathbf{t}_m^T\left[\frac{\bar{\rho}\bar{A}}{\rho}\nabla p + \bar{\mathbf{L}}^{(p)} + \bar{\rho}\bar{A}\frac{\partial}{\partial t}\bar{\mathbf{w}}^{(p)} + \int_{\bar{\mathcal{P}}}(p\mathbf{n})(\hat{\theta},\mathbf{s},t)\,d\hat{\theta}\right]$$

AMP Pressure Condition (normal component of AMP condition)

$$\mathbf{n}^T\int_{\bar{\mathcal{P}}}(p\mathbf{n})(\hat{\theta},\mathbf{s},t)\,d\hat{\theta} + \frac{\bar{\rho}\bar{A}}{\rho}\frac{\partial p}{\partial n} = \mathbf{n}^T\left[-\bar{\mathbf{L}}^{(p)} - \bar{\rho}\bar{A}\frac{\partial}{\partial t}\bar{\mathbf{w}}^{(p)} + \frac{\mu\bar{\rho}\bar{A}}{\rho}\Delta\mathbf{v} + \int_{\bar{\mathcal{P}}}(\boldsymbol{\tau}\mathbf{n})(\hat{\theta},\mathbf{s},t)\,d\hat{\theta}\right]$$

AMP Scheme

We focus on 2D fluid interacts with Euler-Bernoulli Beam for today.

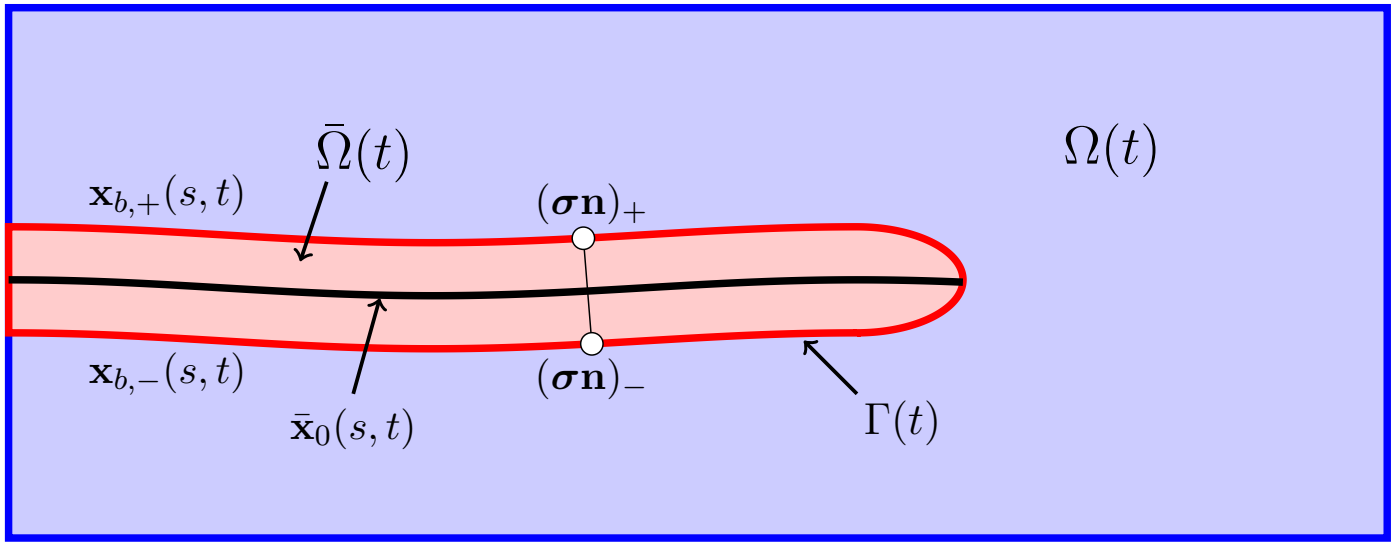

AMP Condition for 2D FSI

$$(\boldsymbol{\sigma}\mathbf{n})_+ + (\boldsymbol{\sigma}\mathbf{n})_- + \frac{\bar{\rho}\bar{h}}{\rho}\nabla\cdot\boldsymbol{\sigma}(\bar{\mathbf{x}}_\pm(s,t),t) = \bar{\mathbf{L}}(\bar{\mathbf{u}}^{(p)},\bar{\mathbf{v}}^{(p)}) + \bar{\rho}\bar{h}\frac{\partial}{\partial t}\bar{\mathbf{w}}_\pm^{(p)}(s,t)$$

Euler-Bernoulli Beam Model

$$\bar{\rho}\bar{h}\frac{\partial^2\eta}{\partial t^2} = -\bar{K}_0\eta + \frac{\partial}{\partial s}\left(\bar{T}\frac{\partial\eta}{\partial s}\right) - \frac{\partial^2}{\partial s^2}\left(\bar{E}\bar{I}\frac{\partial^2\eta}{\partial s^2}\right) - \bar{K}_1\frac{\partial\eta}{\partial t} + \bar{T}_1\frac{\partial^2}{\partial s^2}\left(\frac{\partial\eta}{\partial t}\right) + f(s,t)$$

Deforming Composite Grids (DCG)

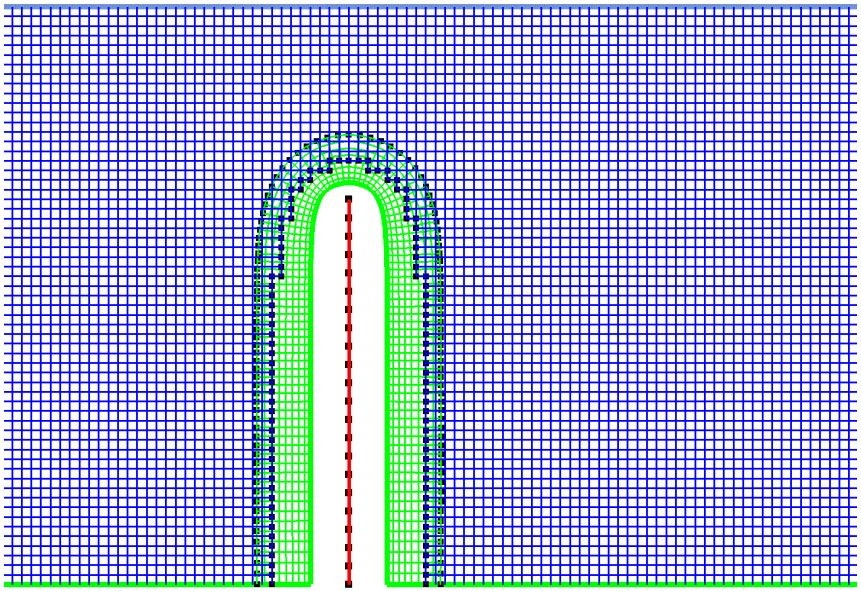

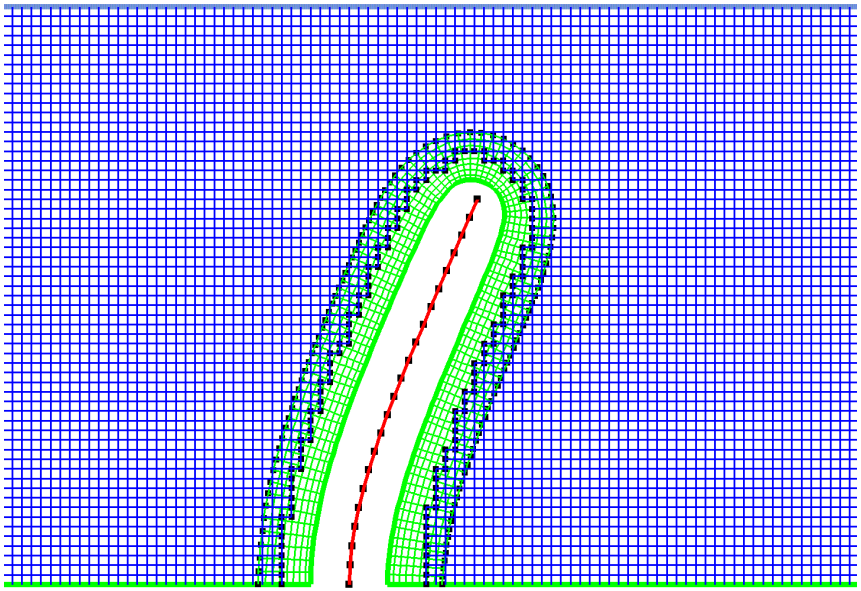

- Composite grids consist of a set of structured component grids that cover the domain and overlap where the component grids meet
- Each component grid is a logically rectangular curvilinear grid
- Solutions on different component grids are coupled by interpolation
- The green fluid grid deforms over time to match the evolving beam (shown in white) and overlaps with the background Cartesian fluid grid (shown in blue)
- The reference curve of the beam is shown in red

Deforming Composite Grids (DCG)

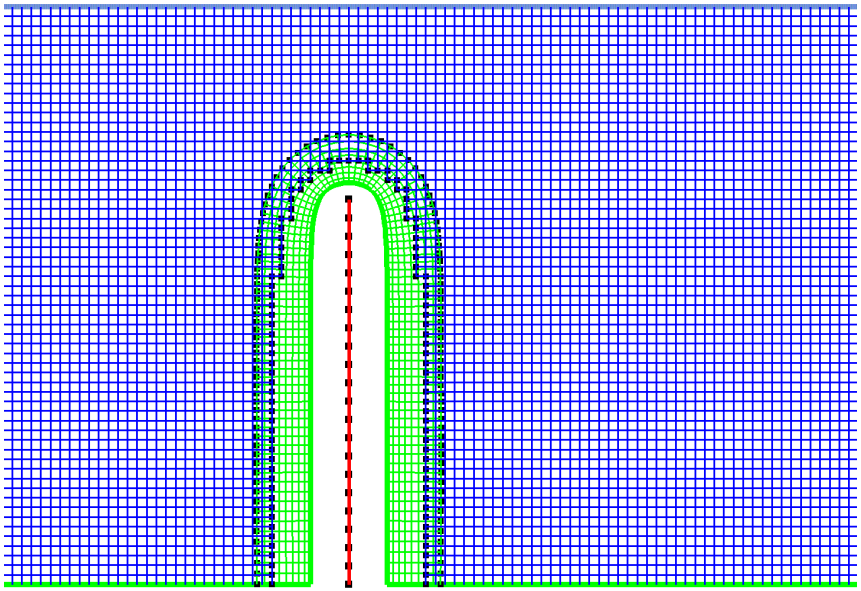

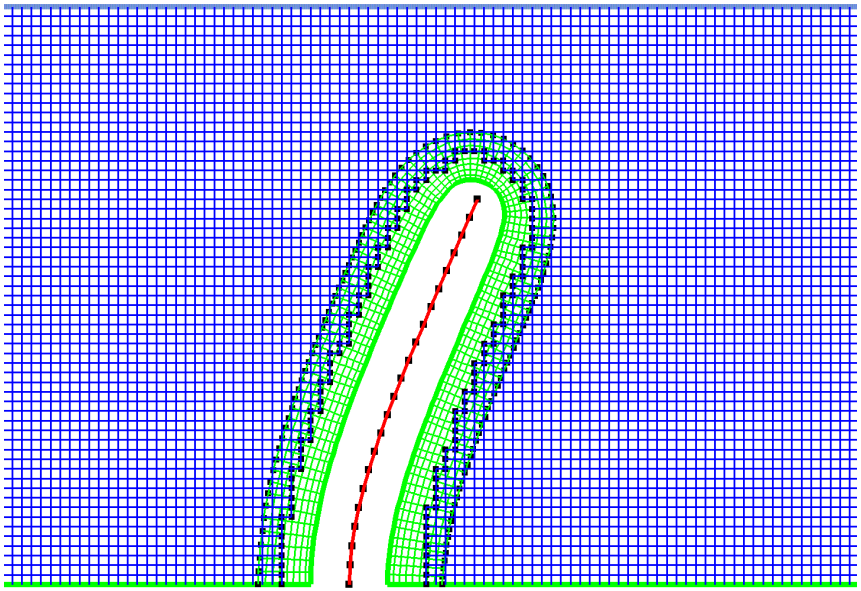

- Composite grids consist of a set of structured component grids that cover the domain and overlap where the component grids meet
- Each component grid is a logically rectangular curvilinear grid
- Solutions on different component grids are coupled by interpolation
- The green fluid grid deforms over time to match the evolving beam (shown in white) and overlaps with the background Cartesian fluid grid (shown in blue)
- The reference curve of the beam is shown in red

Deforming Composite Grids (DCG)

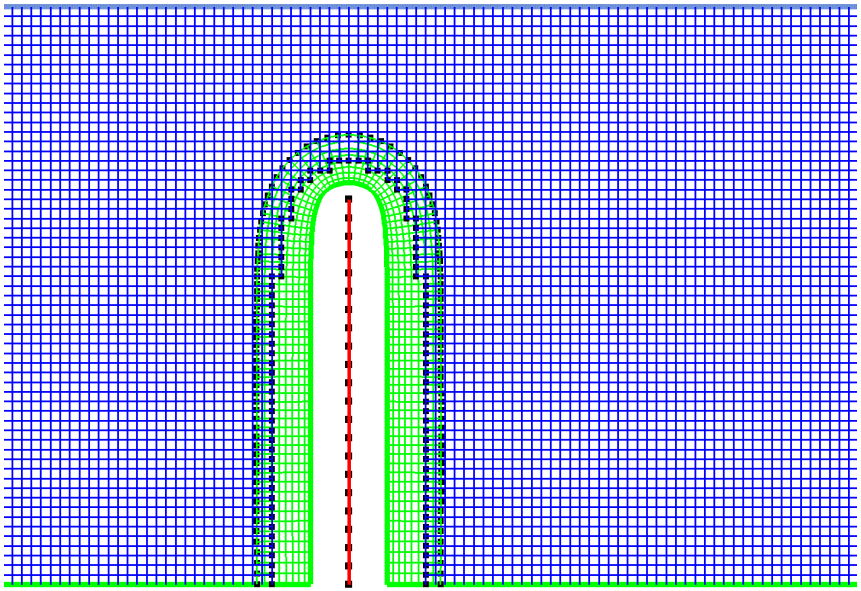

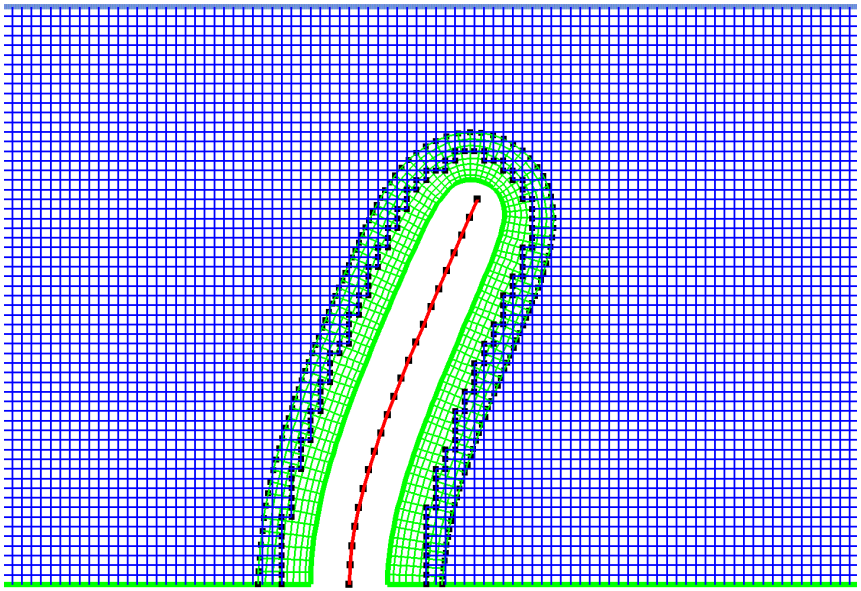

- Composite grids consist of a set of structured component grids that cover the domain and overlap where the component grids meet
- Each component grid is a logically rectangular curvilinear grid
- Solutions on different component grids are coupled by interpolation
- The green fluid grid deforms over time to match the evolving beam (shown in white) and overlaps with the background Cartesian fluid grid (shown in blue)
- The reference curve of the beam is shown in red

Deforming Composite Grids (DCG)

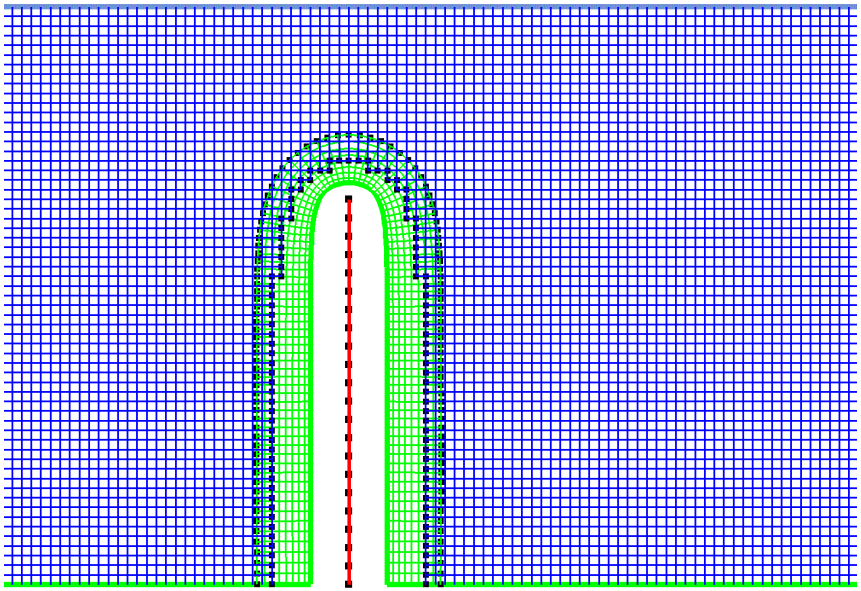

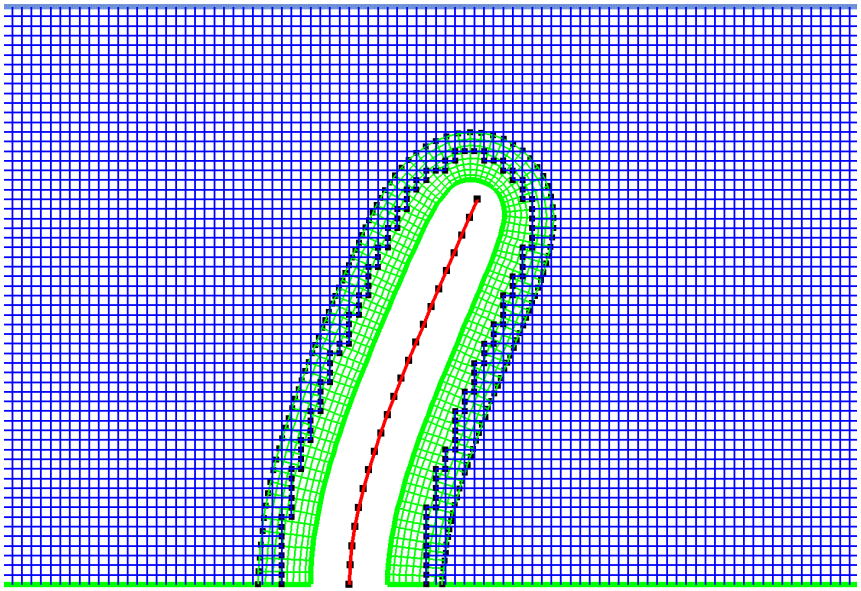

- Composite grids consist of a set of structured component grids that cover the domain and overlap where the component grids meet
- Each component grid is a logically rectangular curvilinear grid
- Solutions on different component grids are coupled by interpolation
- The green fluid grid deforms over time to match the evolving beam (shown in white) and overlaps with the background Cartesian fluid grid (shown in blue)
- The reference curve of the beam is shown in red

Deforming Composite Grids (DCG)

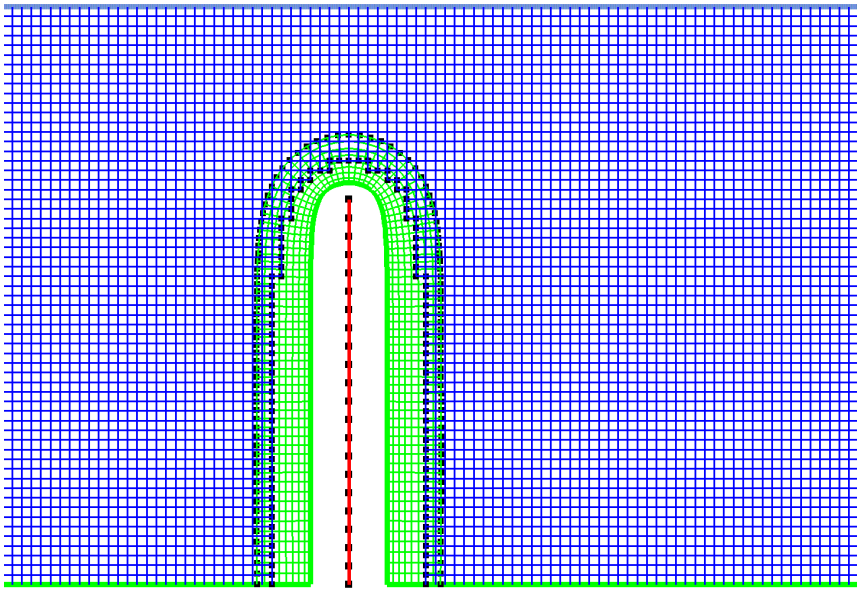

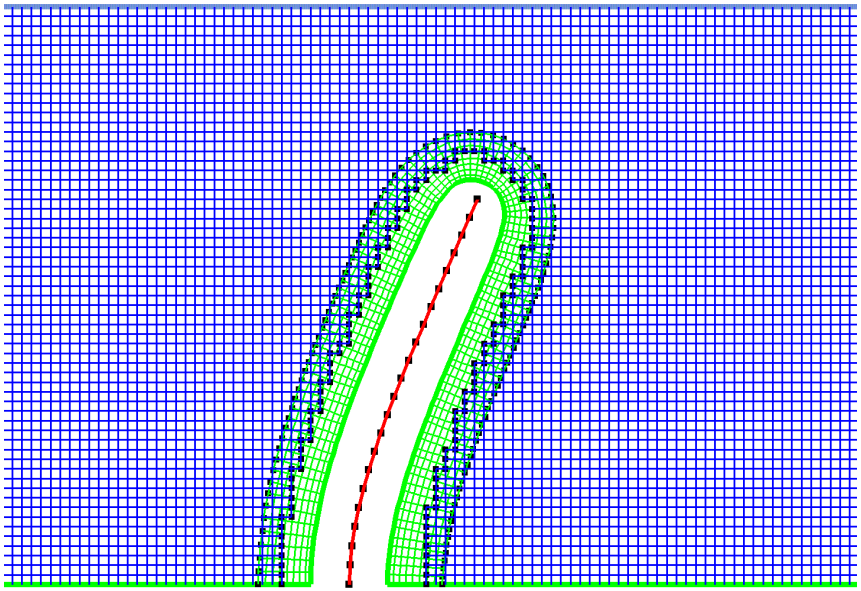

- Composite grids consist of a set of structured component grids that cover the domain and overlap where the component grids meet
- Each component grid is a logically rectangular curvilinear grid
- Solutions on different component grids are coupled by interpolation
- The green fluid grid deforms over time to match the evolving beam (shown in white) and overlaps with the background Cartesian fluid grid (shown in blue)
- The reference curve of the beam is shown in red

Deforming Composite Grids (DCG)

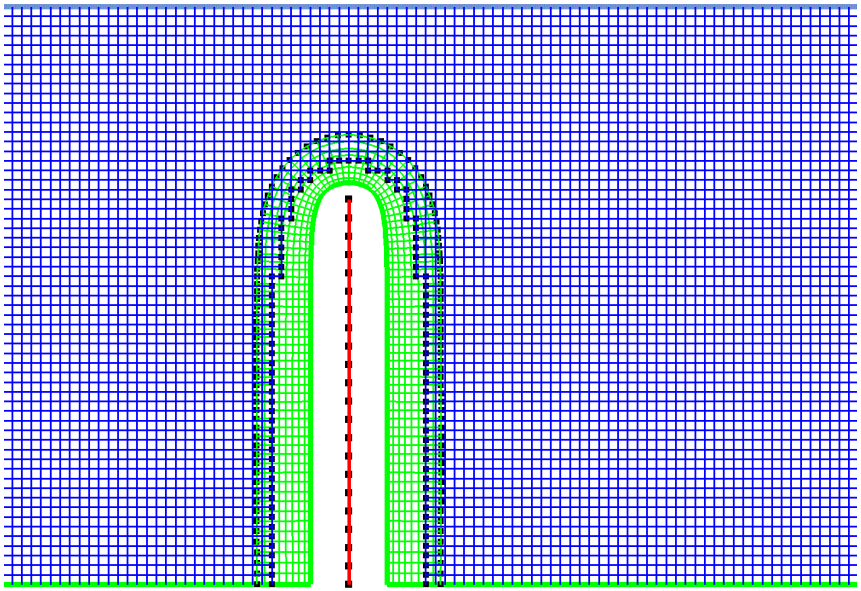

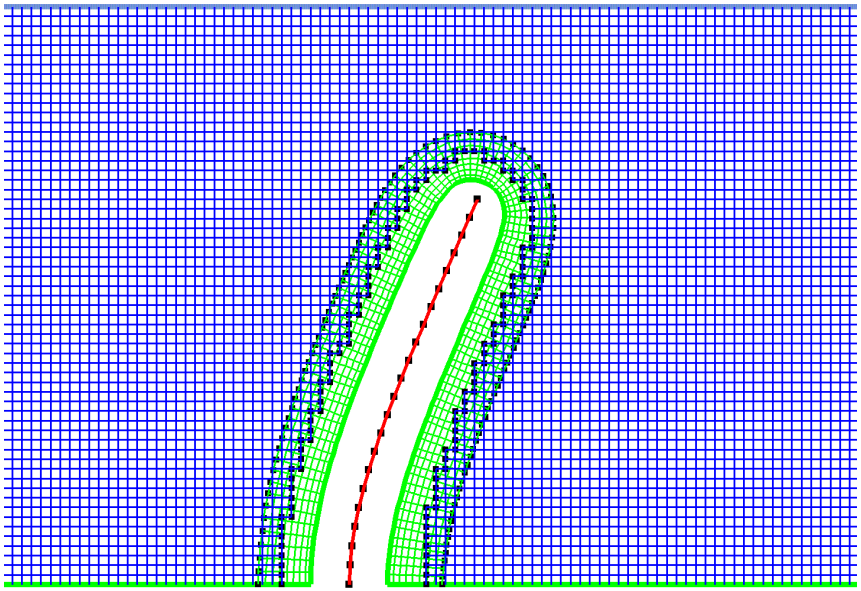

- Composite grids consist of a set of structured component grids that cover the domain and overlap where the component grids meet
- Each component grid is a logically rectangular curvilinear grid
- Solutions on different component grids are coupled by interpolation
- The green fluid grid deforms over time to match the evolving beam (shown in white) and overlaps with the background Cartesian fluid grid (shown in blue)
- The reference curve of the beam is shown in red

Spatial Discretization

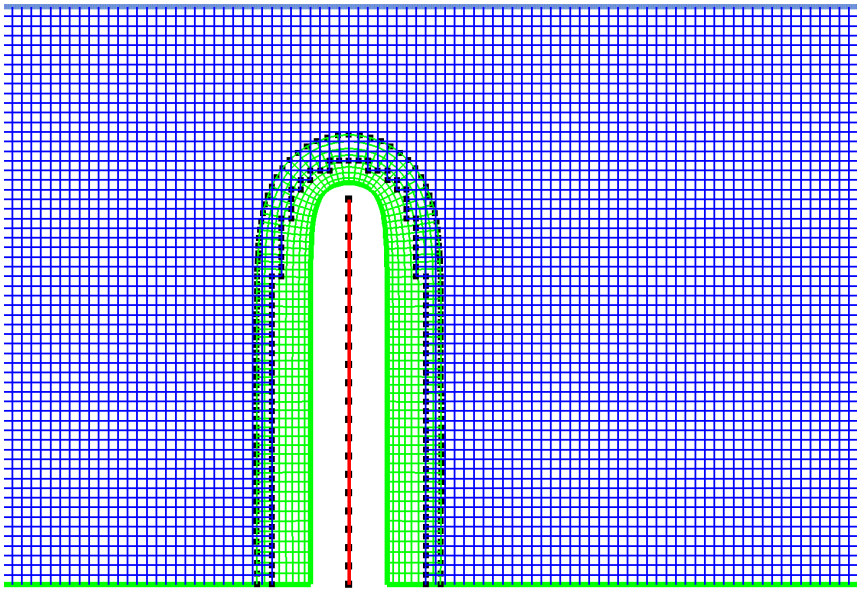

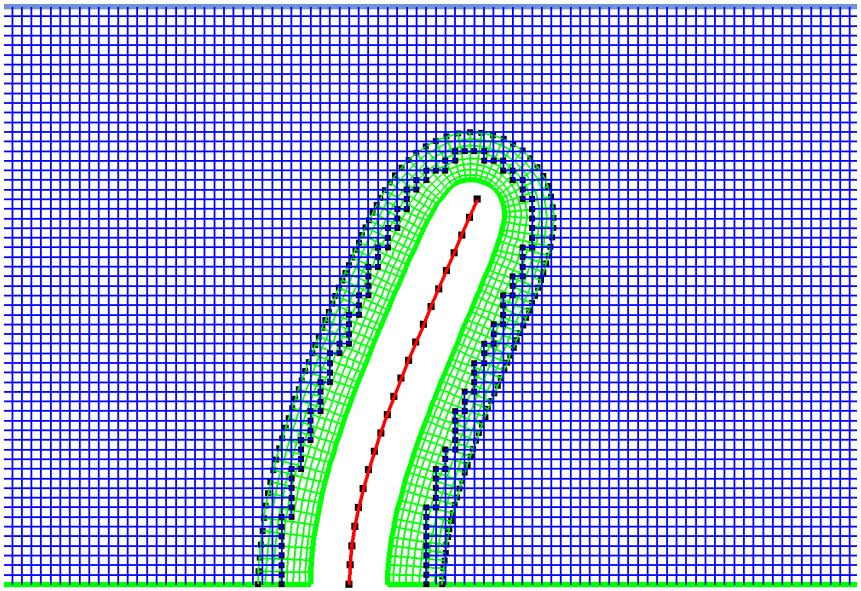

- Fluid equations are discretized using Curvilinear Finite-Difference method in space
- Beam equation is discretized either using Finite-Difference or Finite-Element methods in space

Spatial Discretization

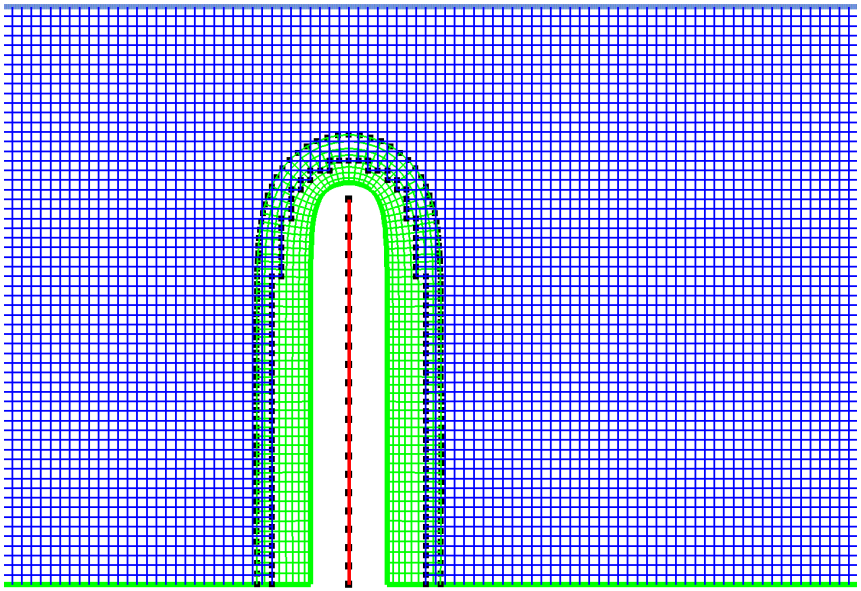

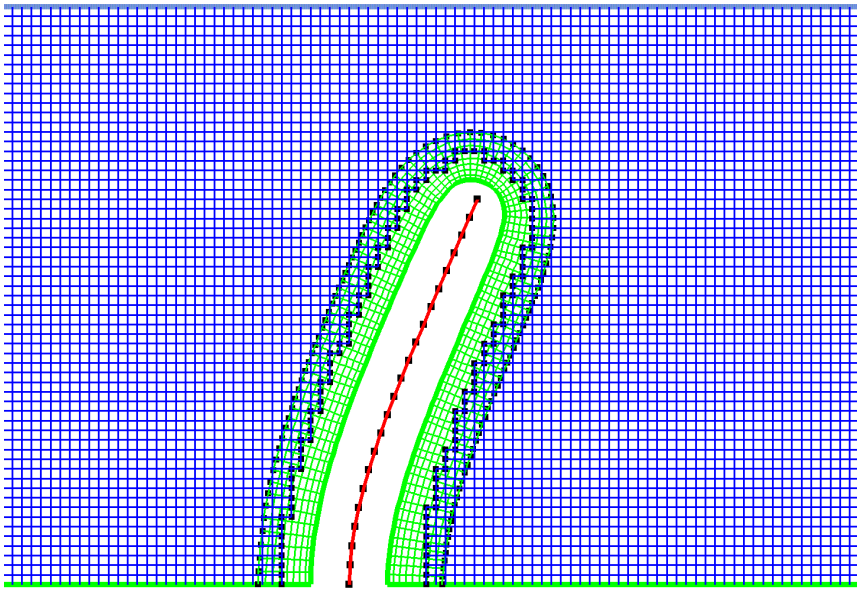

- Fluid equations are discretized using Curvilinear Finite-Difference method in space
- Beam equation is discretized either using Finite-Difference or Finite-Element methods in space

Spatial Discretization

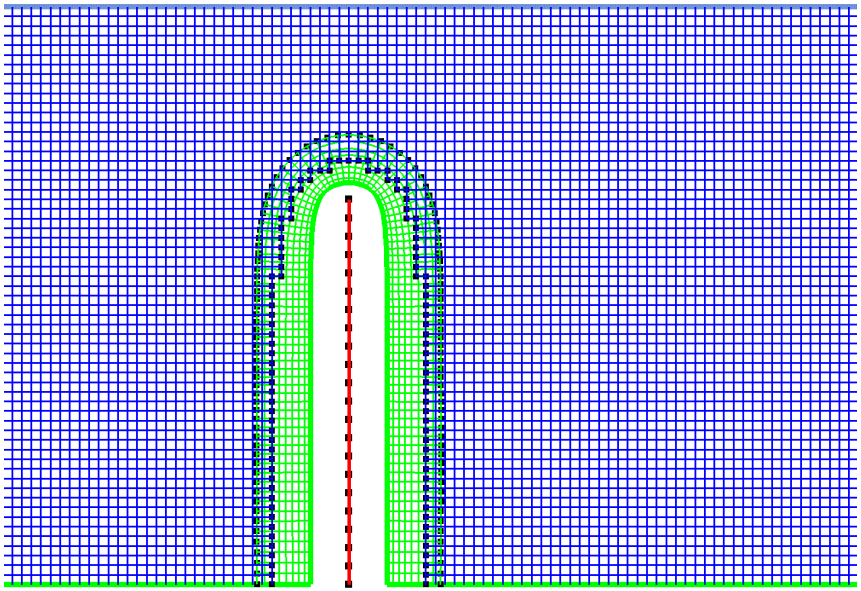

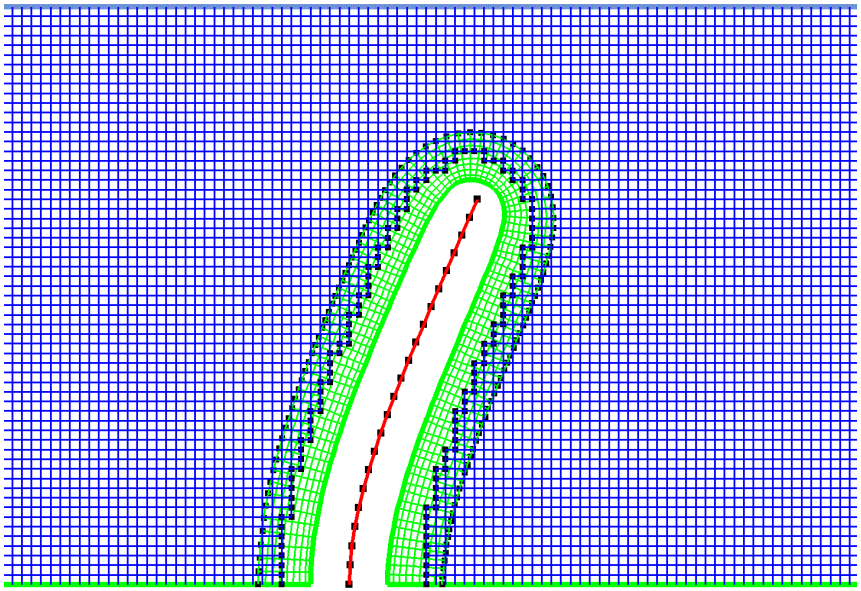

- Fluid equations are discretized using Curvilinear Finite-Difference method in space
- Beam equation is discretized either using Finite-Difference or Finite-Element methods in space

Stability Analysis

Simplified Model

- Inviscid and incompressible fluid on both sides of the beam
- A simple Euler-Bernoulli beam
- Small beam deformation
- Fixed fluid domains
- Periodic boundary conditions in the x.

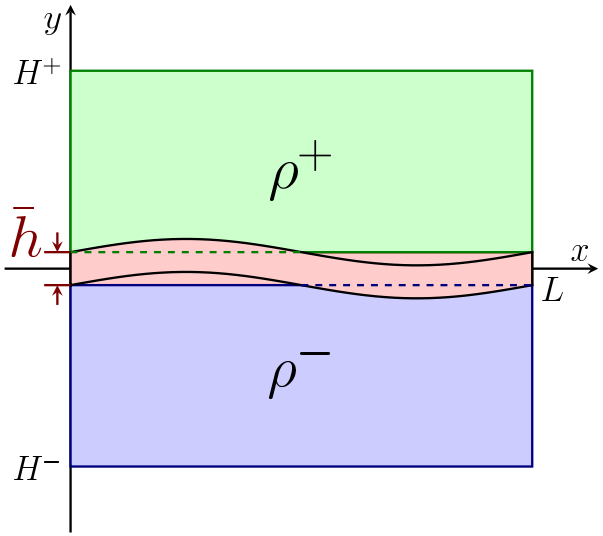

Governing Equations

Fluid:
$$\begin{cases} \rho^{\pm}\dfrac{\partial \mathbf{v}^{\pm}}{\partial t} + \nabla p^{\pm} = 0, & \mathbf{x} \in \Omega_{\pm}, \\ \nabla \cdot \mathbf{v}^{\pm} = 0, & \mathbf{x} \in \Omega_{\pm}, \\ v_2^{\pm}(x, H^{\pm}, t) = 0, & x \in (0, L), \quad \text{Rigid wall} \end{cases}$$

Beam:
$$\begin{cases} \bar{\rho}\bar{h}\dfrac{\partial^2 \eta}{\partial t^2} = -\bar{K}\eta + \bar{T}\dfrac{\partial^2 \eta}{\partial x^2} - \bar{E}\bar{I}\dfrac{\partial^4 \eta}{\partial x^4} + f(x,t), & x \in [0, L], \\ f(x,t) = p^-(x, -\bar{h}/2, t) - p^+(x, +\bar{h}/2, t), \end{cases}$$

Interface:
$$v_2^{\pm}(x, \pm\bar{h}/2, t) = \frac{\partial \eta}{\partial t}(x,t), \qquad x \in [0, L].$$

Stability Analysis

Mode Analysis

The solution can be expressed in terms of a Fourier series in x:

$$\mathbf{v}^{\pm}(x,y,t) \approx \sum_{k=-\infty}^{\infty} \hat{\mathbf{v}}^{\pm}(k,y,t)e^{2\pi ikx/L}, \qquad p^{\pm}(x,y,t) \approx \sum_{k=-\infty}^{\infty} \hat{p}^{\pm}(k,y,t)e^{2\pi ikx/L},$$

and

$$\eta(x,t) = \sum_{k=-\infty}^{\infty} \hat{\eta}(k,t)e^{2\pi ikx/L}.$$

Given Wavenumber k

$$\text{Fluid:} \quad \begin{cases} \rho^{\pm}\dfrac{\partial \hat{v}_1^{\pm}}{\partial t} + ik_x\hat{p}^{\pm} = 0 \\ \rho^{\pm}\dfrac{\partial \hat{v}_2^{\pm}}{\partial t} + \dfrac{\partial \hat{p}^{\pm}}{\partial y} = 0 \\ \dfrac{\partial^2 \hat{p}^{\pm}}{\partial y^2} - k_x^2\hat{p}^{\pm} = 0 \end{cases},$$

$$\text{Beam:} \quad \bar{\rho}\bar{h}\frac{\partial^2\hat{\eta}}{\partial t^2} = -\tilde{L}\hat{\eta} + \hat{p}^{-}(k,-\bar{h}/2,t) - \hat{p}^{+}(k,\bar{h}/2,t),$$

$$\text{Fluid BC:} \quad \frac{\partial \hat{p}^{\pm}}{\partial y}(k,H^{\pm},t) = 0,$$

$$\text{Interface BC:} \quad \hat{v}_2^{\pm}(k,\pm\bar{h}/2,t) = \frac{\partial\hat{\eta}}{\partial t}(k,t)$$

$$\Rightarrow \quad \frac{\partial \hat{p}^{\pm}}{\partial y}(k,\pm\bar{h}/2,t) = -\rho^{\pm}\frac{\partial^2\hat{\eta}}{\partial t^2}(k,t),$$

where $\hat{\mathbf{v}} = (\hat{v}_1, \hat{v}_2)$, $k_x = 2\pi k/L$ and $\tilde{L} = \bar{K} + \bar{T}k_x^2 + \bar{E}\bar{I}k_x^4$.

Stability Analysis

Mode Analysis

The solution can be expressed in terms of a Fourier series in x:

$$\mathbf{v}^{\pm}(x,y,t) \approx \sum_{k=-\infty}^{\infty} \hat{\mathbf{v}}^{\pm}(k,y,t)e^{2\pi ikx/L}, \qquad p^{\pm}(x,y,t) \approx \sum_{k=-\infty}^{\infty} \hat{p}^{\pm}(k,y,t)e^{2\pi ikx/L},$$

and

$$\eta(x,t) = \sum_{k=-\infty}^{\infty} \hat{\eta}(k,t)e^{2\pi ikx/L}.$$

Given Wavenumber k

Fluid:
$$\begin{cases} \rho^{\pm}\dfrac{\partial \hat{v}_1^{\pm}}{\partial t} + ik_x\hat{p}^{\pm} = 0 \\ \rho^{\pm}\dfrac{\partial \hat{v}_2^{\pm}}{\partial t} + \dfrac{\partial \hat{p}^{\pm}}{\partial y} = 0 \\ \dfrac{\partial^2 \hat{p}^{\pm}}{\partial y^2} - k_x^2\hat{p}^{\pm} = 0 \end{cases},$$

Beam: $$\bar{\rho}\bar{h}\frac{\partial^2\hat{\eta}}{\partial t^2} = -\tilde{L}\hat{\eta} + \hat{p}^{-}(k,-\bar{h}/2,t) - \hat{p}^{+}(k,\bar{h}/2,t),$$

Fluid BC: $$\frac{\partial \hat{p}^{\pm}}{\partial y}(k,H^{\pm},t) = 0,$$

Interface BC: $$\hat{v}_2^{\pm}(k,\pm\bar{h}/2,t) = \frac{\partial\hat{\eta}}{\partial t}(k,t)$$

$$\Rightarrow \quad \frac{\partial \hat{p}^{\pm}}{\partial y}(k,\pm\bar{h}/2,t) = -\rho^{\pm}\frac{\partial^2\hat{\eta}}{\partial t^2}(k,t),$$

where $\hat{\mathbf{v}} = (\hat{v}_1, \hat{v}_2)$, $k_x = 2\pi k/L$ and $\tilde{L} = \bar{K} + \bar{T}k_x^2 + \bar{E}\bar{I}k_x^4$.

Added-Mass Coefficients

$$\left(\bar{\rho}\bar{h} + \hat{M}_a^-(k) + \hat{M}_a^+(k)\right)\frac{\partial^2\hat{\eta}}{\partial t^2} = -\tilde{L}\hat{\eta},$$

where

$$\hat{M}_a^{\pm} = \rho^{\pm}\mathcal{D}^{\pm}\left[\frac{\coth(k_x\mathcal{D}^{\pm})}{k_x\mathcal{D}^{\pm}}\right],$$

and $\mathcal{D}^{\pm} = \pm H^{\pm} - \bar{h}/2$ are the depths of the lower and upper fluid domains.

- $\rho^{\pm}\mathcal{D}$ represents the total mass of fluid in the upper and lower domains.
- $\hat{M}_a^{\pm} \to \infty$ as $|k_x\mathcal{D}^{\pm}| \to 0$, added-mass effect is large for low-frequency modes and slender fluid domains.

Stability Analysis

Partitioned Scheme

Stage I: Advance the beam displacement using a leap-frog scheme,

$$\bar{\rho}\bar{h}D_{+t}D_{-t}\hat{\eta}^n = -\tilde{L}\hat{\eta}^n + \hat{p}^{n-}(k,-\bar{h}/2) - \hat{p}^{n+}(k,\bar{h}/2).$$

Stage II: Advance the fluid velocity and pressure using a backward-Euler scheme,

$$\left.\begin{aligned} \rho^{\pm}\frac{\hat{v}_1^{(n+1)\pm} - \hat{v}_1^{n\pm}}{\Delta t} + ik_x\hat{p}^{(n+1)\pm} &= 0 \\ \rho^{\pm}\frac{\hat{v}_2^{(n+1)\pm} - \hat{v}_2^{n\pm}}{\Delta t} + \frac{\partial\hat{p}^{(n+1)\pm}}{\partial y} &= 0 \\ \frac{\partial^2\hat{p}^{(n+1)\pm}}{\partial y^2} - k_x^2\hat{p}^{(n+1)\pm} &= 0 \end{aligned}\right\}, \qquad \begin{aligned} &y \in (H^-, -\tfrac{\bar{h}}{2}) \text{ for the lower fluid,} \\ &y \in (\tfrac{\bar{h}}{2}, H^+) \text{ for the upper fluid,} \end{aligned}$$

At the fluid boundaries:

$$\frac{\partial\hat{p}^{(n+1)\pm}}{\partial y}(k,H^{\pm}) = 0,$$

At the interface:

AMP:

$$\hat{p}^{(n+1)-}(k,-\bar{h}/2) - \hat{p}^{(n+1)+}(k,+\bar{h}/2) + \frac{\bar{\rho}\bar{h}}{\rho^{\pm}}\frac{\partial\hat{p}^{(n+1)\pm}}{\partial y}(k,\pm\bar{h}/2) = \tilde{L}\hat{\eta}^{n+1}(k).$$

TP:

$$\hat{v}_2^{(n+1)\pm}(k,\pm\bar{h}/2) = D_{-t}\hat{\eta}^{n+1}(k).$$

Stability Analysis

Partitioned Scheme

Stage I: Advance the beam displacement using a leap-frog scheme,

$$\bar{\rho}\bar{h}D_{+t}D_{-t}\hat{\eta}^n = -\tilde{L}\hat{\eta}^n + \hat{p}^{n-}(k,-\bar{h}/2) - \hat{p}^{n+}(k,\bar{h}/2).$$

Stage II: Advance the fluid velocity and pressure using a backward-Euler scheme,

$$\left.\begin{aligned} \rho^{\pm}\frac{\hat{v}_1^{(n+1)\pm} - \hat{v}_1^{n\pm}}{\Delta t} + ik_x\hat{p}^{(n+1)\pm} &= 0 \\ \rho^{\pm}\frac{\hat{v}_2^{(n+1)\pm} - \hat{v}_2^{n\pm}}{\Delta t} + \frac{\partial\hat{p}^{(n+1)\pm}}{\partial y} &= 0 \\ \frac{\partial^2\hat{p}^{(n+1)\pm}}{\partial y^2} - k_x^2\hat{p}^{(n+1)\pm} &= 0 \end{aligned}\right\}, \qquad \begin{aligned} &y \in (H^-, -\tfrac{\bar{h}}{2}) \text{ for the lower fluid,} \\ &y \in (\tfrac{\bar{h}}{2}, H^+) \text{ for the upper fluid,} \end{aligned}$$

At the fluid boundaries:

$$\frac{\partial\hat{p}^{(n+1)\pm}}{\partial y}(k,H^{\pm}) = 0,$$

At the interface:

AMP:

$$\hat{p}^{(n+1)-}(k,-\bar{h}/2) - \hat{p}^{(n+1)+}(k,+\bar{h}/2) + \frac{\bar{\rho}\bar{h}}{\rho^{\pm}}\frac{\partial\hat{p}^{(n+1)\pm}}{\partial y}(k,\pm\bar{h}/2) = \tilde{L}\hat{\eta}^{n+1}(k).$$

TP:

$$\hat{v}_2^{(n+1)\pm}(k,\pm\bar{h}/2) = D_{-t}\hat{\eta}^{n+1}(k).$$

Stability Analysis

Theorem

When $k \neq 0$, the AMP Algorithm is stable if and only if

$$\Delta t < 2\sqrt{\frac{\bar{\rho}\bar{h} + \hat{M}_a^+(k) + \hat{M}_a^-(k)}{\tilde{L}}},$$

where $\hat{M}_a^{\pm}(k)$ is the same as before. When $k = 0$, the scheme is non-dissipative.

Theorem

Assuming $\bar{\rho}\bar{h} > 0$ and $\tilde{L} > 0$, the TP Algorithm is weakly stable if and only if

$$\Delta t < 2\sqrt{\frac{\bar{\rho}\bar{h} - \hat{M}_a^-(k) - \hat{M}_a^+(k)}{\tilde{L}}}.$$

- AMP scheme is always stable provided the time step restriction is satisfied.
- For this simple AMP scheme, fluid and beam velocities match to first-order accuracy at the interface.
- An additional projection step could be included to match the interface velocities.
- TP scheme is unconditionally unstable when $\bar{\rho}\bar{h} < \hat{M}_a^-(k) + \hat{M}_a^+(k)$. [Causin *et. al.*, 2005]
- The theorem provides an estimate for time-step when $\bar{\rho}\bar{h} > \hat{M}_a^-(k) + \hat{M}_a^+(k)$.

Numerical Results

Manufactured Solutions

$$u_e(x, y, t) = -a\cos(f_x\pi x)\sin\left(f_x\pi(y-\eta_e-1)\right)\cos(f_t\pi t),$$

$$v_e(x, y, t) = a\sin(f_x\pi x)\cos\left(f_x\pi(y-\eta_e-1)\right)\cos(f_t\pi t) - a\cos(f_x\pi x)\sin\left(f_x\pi(y-\eta)\right)\frac{\partial\eta_e}{\partial x}\cos(f_t\pi t),$$

$$p_e(x, y, t) = \cos(f_x\pi x)\cos(f_x\pi y)\cos(f_t\pi t),$$

$$\eta_e(x, t) = \frac{a}{\pi f_t}\sin(f_x\pi x)\sin(f_t\pi t).$$

- The exact solution is divergence free.
- Fluid and Beam velocities match at the interface.

Deforming Grids

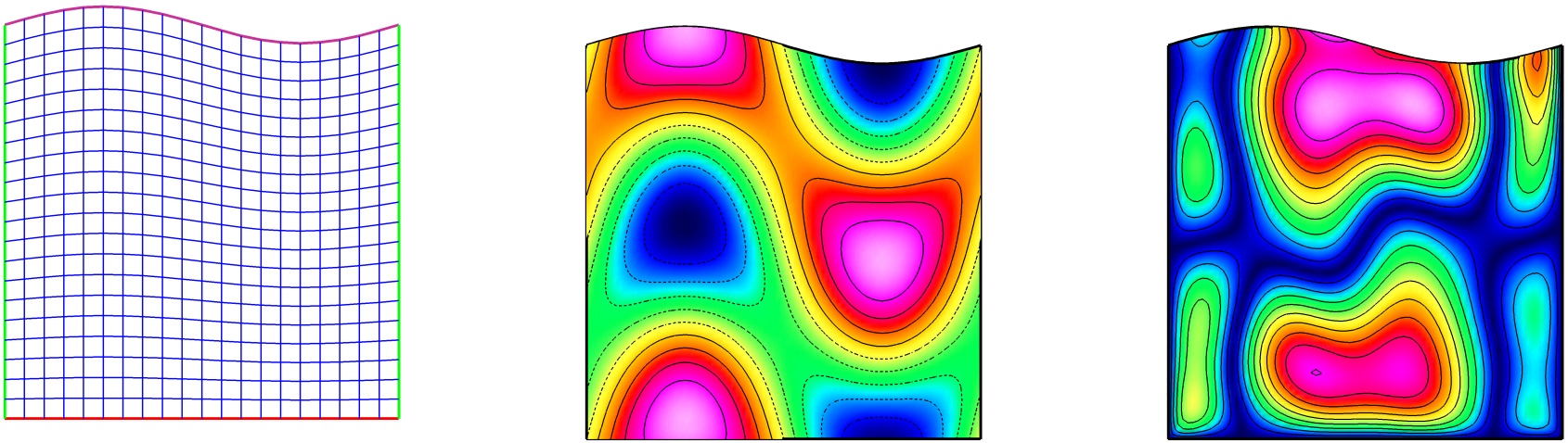

Figure: Computational results at $t = 0.1$ for a light beam ($\bar{\rho}\bar{h} = 10^{-3}$)

Numerical Results

light beam, $\bar{\rho}\bar{h} = 10^{-3}$										
h_j	$E_j^{(p)}$	r	$E_j^{(v_1)}$	r	$E_j^{(v_2)}$	r	$E_j^{(\eta)}$	r	$E_j^{(\eta_t)}$	r
1/10	6.55e-02		2.64e-02		2.23e-02		9.06e-04		2.19e-02	
1/20	1.70e-02	3.84	7.26e-03	3.64	5.41e-03	4.12	2.23e-04	4.07	5.15e-03	4.25
1/40	4.45e-03	3.83	1.86e-03	3.91	1.39e-03	3.90	6.03e-05	3.69	1.31e-03	3.94
1/80	1.12e-03	3.98	4.70e-04	3.95	3.55e-04	3.91	1.54e-05	3.90	3.29e-04	3.97
rate	1.96		1.94		1.99		1.95		2.01	
medium beam, $\bar{\rho}\bar{h} = 1$										
h_j	$E_j^{(p)}$	r	$E_j^{(v_1)}$	r	$E_j^{(v_2)}$	r	$E_j^{(\eta)}$	r	$E_j^{(\eta_t)}$	r
1/10	1.18e-01		2.07e-02		2.40e-02		3.56e-04		9.09e-03	
1/20	2.53e-02	4.69	5.86e-03	3.53	5.80e-03	4.14	7.70e-05	4.63	1.89e-03	4.80
1/40	6.49e-03	3.90	1.54e-03	3.80	1.52e-03	3.82	2.02e-05	3.81	4.61e-04	4.11
1/80	1.67e-03	3.89	3.95e-04	3.90	3.87e-04	3.92	5.10e-06	3.96	1.15e-04	4.02
rate	2.04		1.91		1.98		2.03		2.10	
heavy beam, $\bar{\rho}\bar{h} = 10^{3}$										
h_j	$E_j^{(p)}$	r	$E_j^{(v_1)}$	r	$E_j^{(v_2)}$	r	$E_j^{(\eta)}$	r	$E_j^{(\eta_t)}$	r
1/10	1.73e-01		2.06e-02		2.80e-02		8.45e-05		2.91e-03	
1/20	3.33e-02	5.20	5.63e-03	3.66	6.68e-03	4.20	2.25e-05	3.76	7.72e-04	3.77
1/40	8.83e-03	3.77	1.51e-03	3.74	1.77e-03	3.77	6.37e-06	3.53	1.91e-04	4.05
1/80	2.31e-03	3.82	3.90e-04	3.86	4.54e-04	3.90	1.63e-06	3.92	4.75e-05	4.01
rate	2.06		1.91		1.98		1.89		1.98	

Figure: Maximum-norm errors and estimated convergence rates using manufactured solutions. The column labeled “r” provides the ratio of the errors at the current grid spacing to that on the next coarser grid.

Numerical Results

Beam Under Pressure

Exact steady-state solutions:

$$u^{\pm} = 0,\ v^{\pm} = 0,\ p^{-} = p_a,\ p^{+} = p_b,\ \text{and}\ \eta = \frac{P_0}{24\bar{E}\bar{I}}\left(1 - s^2\right)^2.$$

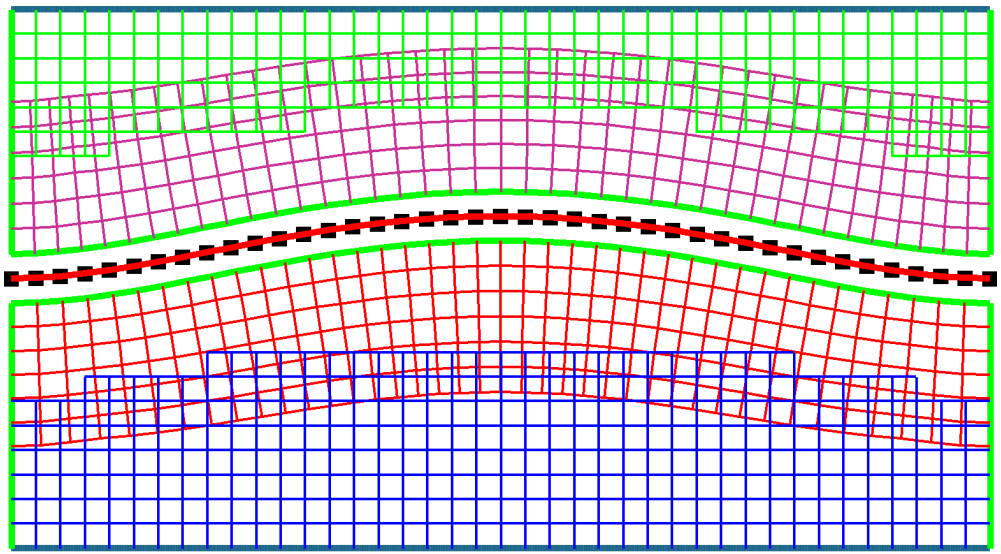

- The problem is solved for beams: $\bar{\rho}\bar{h} = .01, .1, 1, 10$ and 100.
- For all beams, the AMP scheme is stable.
- The solution converges to the exact steady-state solution (up to round-off errors).

Numerical Results

Beam Under Pressure

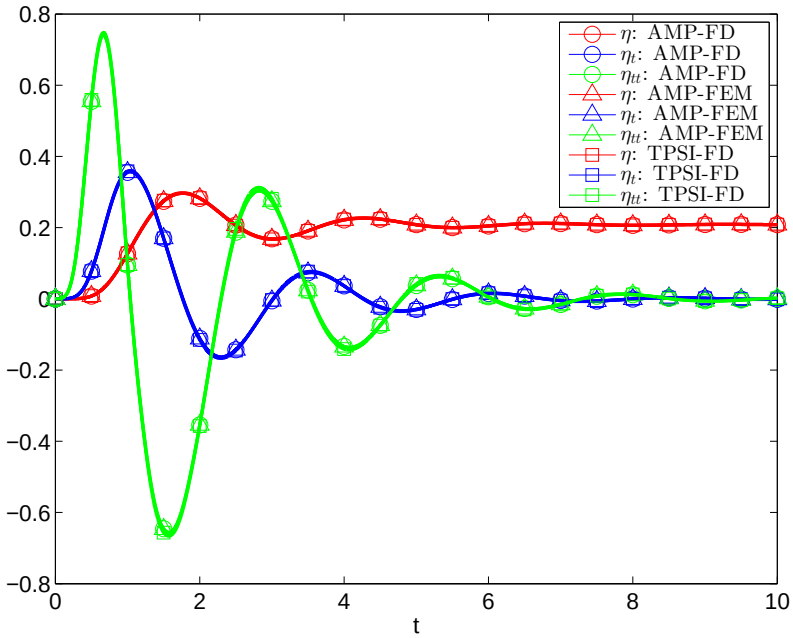

Motion of the beam mid-point for the case $\bar{\rho}\bar{h} = 0.01$

grid	$E_j^{(p)}$	r	$E_j^{(u)}$	r	$E_j^{(v)}$	r
G2	4.7e-4		1.1e-3		7.7e-4	
G4	1.2e-4	4.0	3.1e-4	3.6	2.1e-4	3.7
G8	3.0e-5	4.0	8.5e-5	3.6	5.6e-5	3.7
G16	7.6e-6	4.0	2.3e-5	3.6	1.5e-5	3.7
	1.99		1.86		1.89	

Self convergence results (Richardson extrapolation) at $t = 2.5$ for the case of a heavy ($\bar{\rho}\bar{h} = 100$).

Numerical Results

Pressure-pulse in Elastic Tube

- Top Boundary:
  - Flexible beam
  - AMP Interface conditions
- Left Boundary:
  - Time dependent pressure pulse

$$p(0, y, t) = \begin{cases} p_{\max} \sin(\pi t / t_{\max}) & \text{for } 0 \leq t \leq t_{\max} \\ 0 & \text{for } t > t_{\max} \end{cases}$$

  - Provide tangential velocity: $v_2 = 0$
- Bottom Boundary:
  - Slip-wall: $\mathbf{n}^T \mathbf{v} = 0$ and $\mathbf{t}^T \boldsymbol{\tau} \mathbf{n} = 0$.
- Right Boundary:
  - Outflow: $p = 0$ and $\mathbf{v}$ is extrapolated
- Parameters:
  - Fluid: $\rho = 1$, $\mu = 1.0$
  - Beam: $\bar{\rho} = 1.1$, $\bar{h} = 0.1$, $\bar{E} = 0.25e6$, $\bar{T} = \bar{E}\bar{h}/(2(1+\bar{\nu}))$, $\bar{\nu} = 0.5$, $\bar{K}_0 = \bar{E}\bar{h}/(R^2(1-\bar{\nu}^2))$, $\bar{K}_t = \bar{\rho}\bar{h}$, and $\bar{K}_{xxt} = 10^{-3}\bar{T}$ (visco-elastic damping)

Note

TP scheme needs 20 sub-iterations on average.

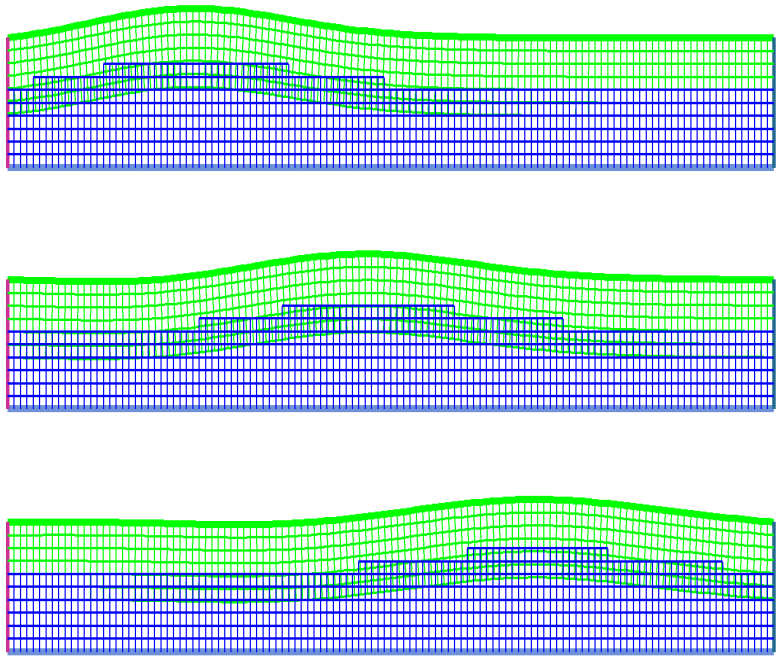

Figure: At $t = 0.010$, 0.015 and 0.020.

Numerical Results

Pressure-pulse in Elastic Tube

- Top Boundary:
  - Flexible beam
  - AMP Interface conditions
- Left Boundary:
  - Time dependent pressure pulse

$$p(0, y, t) = \begin{cases} p_{\max} \sin(\pi t / t_{\max}) & \text{for } 0 \leq t \leq t_{\max} \\ 0 & \text{for } t > t_{\max} \end{cases}$$

  - Provide tangential velocity: $v_2 = 0$
- Bottom Boundary:
  - Slip-wall: $\mathbf{n}^T \mathbf{v} = 0$ and $\mathbf{t}^T \boldsymbol{\tau} \mathbf{n} = 0$.
- Right Boundary:
  - Outflow: $p = 0$ and $\mathbf{v}$ is extrapolated
- Parameters:
  - Fluid: $\rho = 1$, $\mu = 1.0$
  - Beam: $\bar{\rho} = 1.1$, $\bar{h} = 0.1$, $\bar{E} = 0.25e6$, $\bar{T} = \bar{E}\bar{h}/(2(1+\bar{\nu}))$, $\bar{\nu} = 0.5$, $\bar{K}_0 = \bar{E}\bar{h}/(R^2(1-\bar{\nu}^2))$, $\bar{K}_t = \bar{\rho}\bar{h}$, and $\bar{K}_{xxt} = 10^{-3}\bar{T}$ (visco-elastic damping)

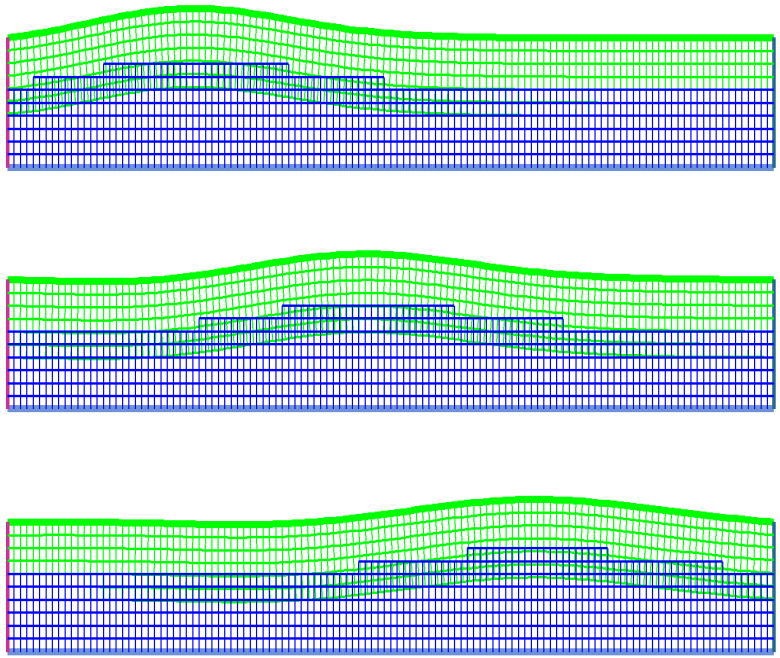

Figure: At $t = 0.010$, 0.015 and 0.020.

Note

TP scheme needs 20 sub-iterations on average.

Numerical Results

Pressure-pulse in Elastic Tube

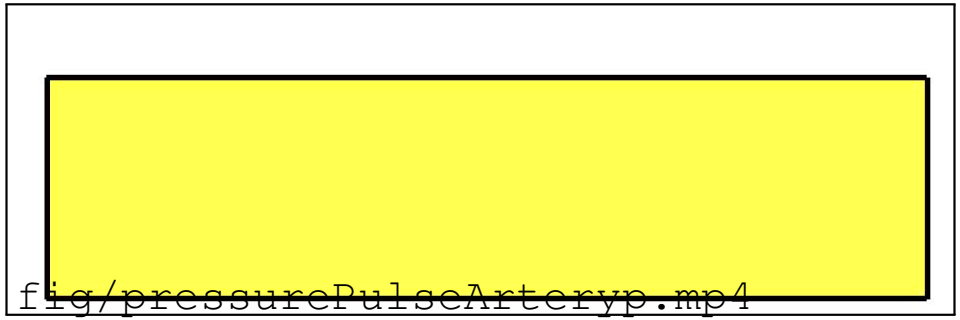

Pressure p

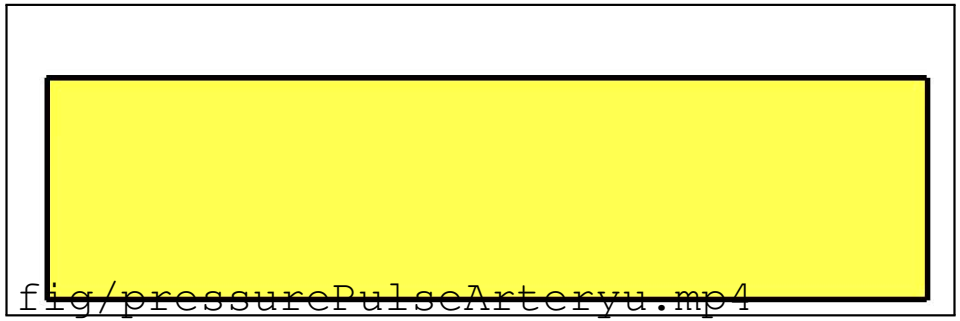

Velocity v_1

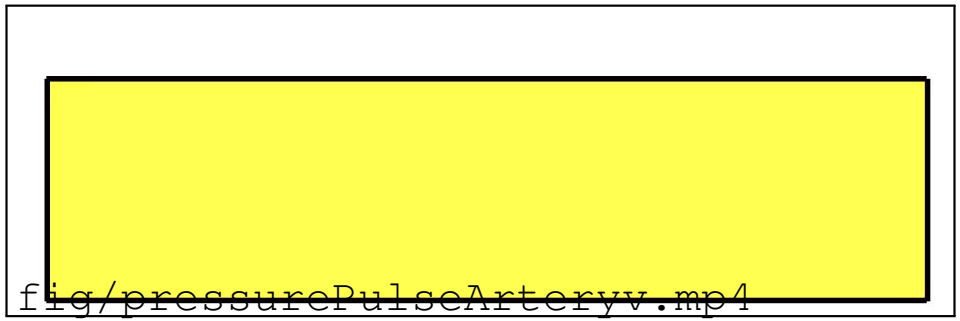

Velocity v_2

Numerical Results

Four Beams in A channel

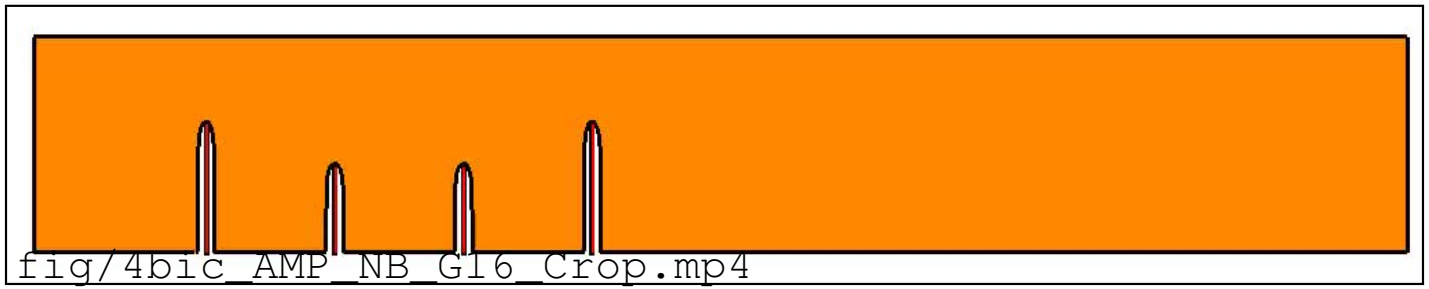

Computed using grid $G^{(16)}$ (760K grid points).

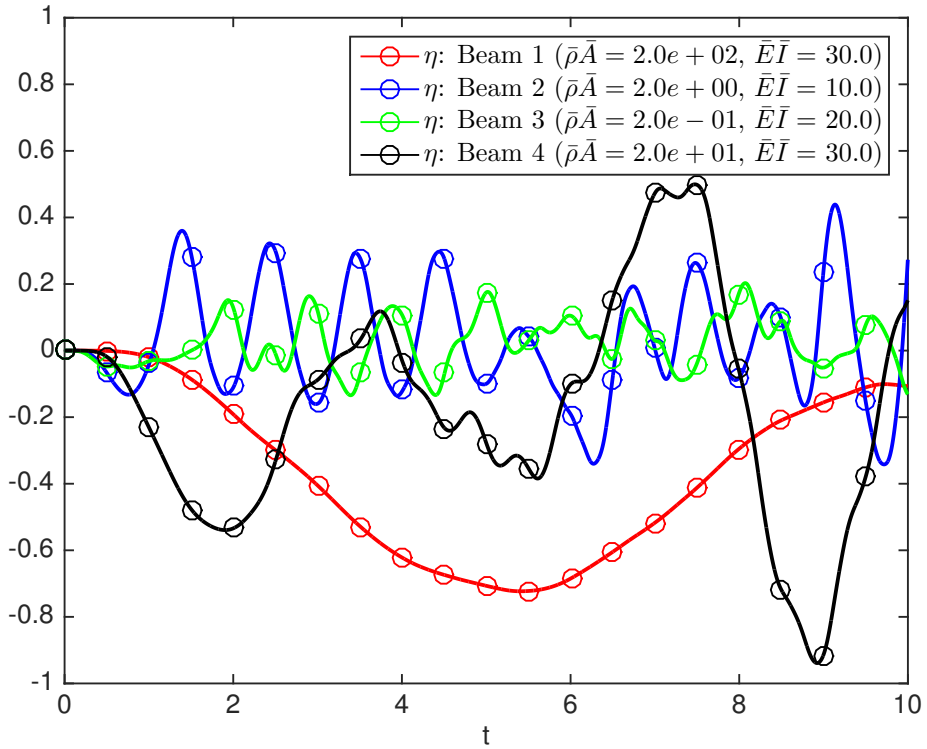

Beam tip motions

Numerical Results

Run-time performance of AMP versus TP-SI				
	AMP	TP-SI		AMP speed-up
	s/step	s/step	sub-its	TP-SI/AMP
$\bar{\rho} = 1$	2.87	22.6	62	7.87
$\bar{\rho} = 100$	1.33	1.48	0	1.1

Figure: Comparison of the run-time performance of the AMP scheme versus the TP-SI scheme for flow past a light and heavy beam in a channel computed using grid $G^{(8)}$ (150K grid points).

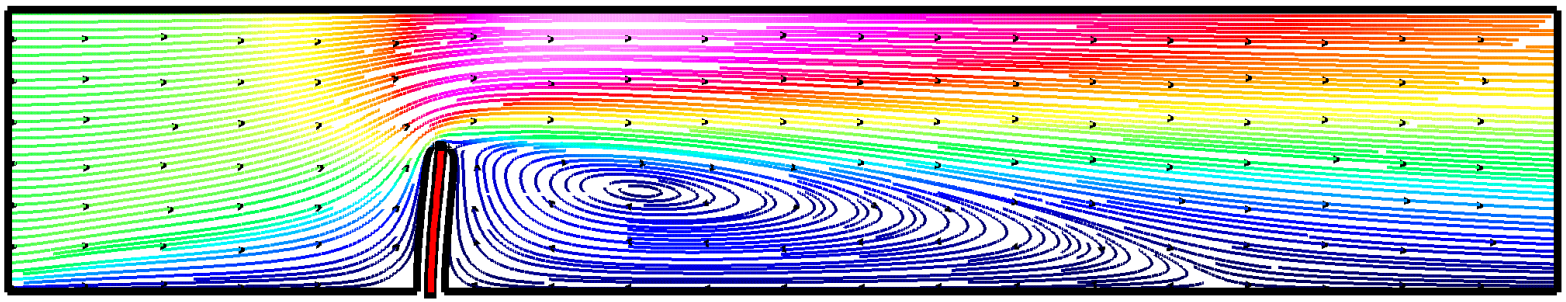

Summary

Conclusion

- We extended the AMP algorithm for linearized problems to the nonlinear regime.
- We conducted mode analysis for the TP and the AMP schemes using a simplified model with fluids on both sides of the beam:
  - TP scheme is unconditionally unstable for light beam,
  - AMP scheme is always stable.
- We implemented the AMP scheme for INS+BEAM problems on deforming domains; large deformations are handled using deforming composite grids.
- Numerical evidence reveals second-order accuracy for the AMP scheme.

Future Work

- Develop and analyze high-order AMP algorithms.
- Extend the AMP algorithms for 3D FSI problems.
- Apply the AMP algorithms to interesting applications; for example, blood flow in veins and arteries.

Thank You!